1-28-2021

Stick-Slip Tremor Beneath an Alpine Glacier

J. Umlauft
Leipzig University

F. Lindner
LMU Munich

P. Roux
ISTerre

T. D. Mikesell
Boise State University

M. M. Haney
U.S. Geological Survey

See next page for additional authors

AGU ADVANCING EARTH AND SPACE SCIENCE

Geophysical Research Letters

RESEARCH LETTER
10.1029/2020GL090528

Stick-Slip Tremor Beneath an Alpine Glacier

J. Umlauft[1], F. Lindner[2,3], P. Roux[4], T. D. Mikesell[5], M. M. Haney[6], M. Korn[1], and F. T. Walter[3]

[1]Institute of Geophysics and Geology, Leipzig University, Leipzig, Germany, [2]Department of Earth and Environmental Sciences, LMU Munich, Munich, Germany, [3]ETH Zurich, Laboratory of Hydraulics, Hydrology and Glaciology, Zurich, Switzerland, [4]ISTerre - Maison des Géosciences, Grenoble, France, [5]Department of Geosciences, Environmental Seismology Laboratory, Boise State University, Boise, ID, USA, [6]U.S. Geological Survey, Alaska Volcano Observatory, Anchorage, AK, USA

Key Points:

- We revisit a harmonic tremor recorded by a seismic array on an Alpine glacier, which was previously interpreted as hydraulic tremor
- Applying matched field processing that accounts for nonisotropic radiation patterns suggests a tremor source at the ice-bedrock interface
- A focal mechanism derived from ice slip over bedrock explains our results and suggests seismogenic stick-slip motion at the glacier's base

Supporting Information:

- Supporting Information S1

Correspondence to:
J. Umlauft,
josefine.umlauft@uni-leipzig.de

Citation:
Umlauft, J., Lindner, F., Roux, P., Mikesell, T. D., Haney, M. M., Korn, M., & Walter, F. T. (2021). Stick-slip tremor beneath an Alpine glacier. *Geophysical Research Letters*, *48*, e2020GL090528. https://doi.org/10.1029/2020GL090528

Received 25 AUG 2020
Accepted 4 DEC 2020

Abstract Sliding of glacial ice over its base is typically described by a frictionless or slowly deforming bed. This view is challenged by recent seismic observations of stick-slip motion at the ice-bed interface. We revisit a high-frequency (20–35 Hz) harmonic tremor recorded on Gornergletscher, Switzerland. In contrast to previous interpretation in terms of glaciohydraulic tremor, we present evidence for superimposed stick-slip episodes as tremor sources: we locate the tremor source with matched field processing polarity optimization, which allows for azimuthal polarity patterns associated with nonisotropic moment tensors and yields a tremor source clustering near the glacier bed. Our analysis confirms an *S* wave radiation pattern in agreement with a double-couple source derived from ice sliding over bedrock and explains our tremor observations in terms of glacier stick-slip motion. Adding to observations of stick-slip tremor beneath polar ice streams, this first report on stick-slip tremor beneath Alpine ice favors widespread seismogenic glacier sliding.

Plain Language Summary For many years, researchers have observed cryoseismic stick-slip tremor exclusively in Antarctica. Stick-slip tremor is due to small repeating slip events at the glacier bed as a glacier advances downstream. This type of tremor is a telltale sign of what is happening at the ice-bed interface and indicates frictional sliding. Here, we present first evidence for stick-slip tremor at an Alpine glacier—Gornergletscher, Switzerland. We identify indicators in the seismic signature and apply data processing techniques that reveal that the creeping glacier sole moves under the influence of gravity and irregularly rubs over a sticky area at the bed.

1. Introduction

Sliding of glacial ice over its base is typically the dominant flow mechanism of glaciers and ice sheets. The term "sliding" is often used in a loose sense to include the deformation of "soft" till beds and the differential motion between basal ice and underlying bedrock. The amount of sliding controls fast (Clarke, 1987) and slow (Maier et al., 2019) ice flow regimes. Sliding variations are powerful enough to halt, or even reverse, ice stream flow (Conway et al., 2002) or rupture ice tongues, leading to massive ice avalanches (Faillettaz et al., 2015; Kääb et al., 2018). Nevertheless, sliding mechanisms remain elusive, leading to uncertain predictions of ice sheet motion and stability, and ultimately sea level rise (Alley et al., 2005; Huybrechts, 2002; Meier et al., 2007; Ritz et al., 2015).

The traditional view on basal sliding was introduced by Weertman (1957) who considered a frictionless glacier bed, whose far-field shear resistance arises from normal forces on undeformable bed undulations. Sliding thus occurs via regelation and enhanced deformation around stiff bed obstacles. Later modifications to this theory accounted for water-filled cavities at the lee sides of bed undulations (Gagliardini et al., 2007; Iken, 1981; Schoof, 2005) to explain observed ice flow acceleration in response to melt production (e.g., Bartholomew et al., 2010; Harper et al., 2007; Maier et al., 2019, and references therein). For fast ice stream flow over till beds, a combination of true sliding over the till surface and pervasive till deformation dominate over traditional Weertman-type sliding (Engelhardt & Kamb, 1998; Iverson et al., 2003; Tulaczyk, 1999). As till pore pressures control plastic yield stresses, basal motion for deformable beds also depends on meltwater supply (Bougamont et al., 2014; Iverson, 2010; Walter et al., 2014).

The ideas of frictionless beds or deforming till layers make theoretical descriptions of basal stresses tractable and still influence modern sliding theories (e.g., Schoof, 2005; Zoet & Iverson, 2020). However, in recent years, observations of seismogenesis at the ice-bed interface showed that glacier sliding is not a smooth process at all locations as expected for Weertman-type frictionless sliding or deformable beds. Instead, episodes of sudden glacier slip that emit seismic waves testify to frictional processes, analogous to tectonic faults, and cannot be explained by slow ice regelation and creep or till deformation (overviews on glacial stick-slip motion are given in Podolskiy and Walter [2016] and Aster and Winberry [2017]). Seismic magnitudes of stick-slip events are highly variable, with negative magnitudes corresponding to microseismic earthquakes beneath Alpine glaciers (e.g., Helmstetter et al., 2015; Walter et al., 2020) and up to magnitude seven events beneath Antarctic ice streams (Wiens et al., 2008). Microseismic stick-slip events, in particular, seem to be a widespread and potentially ubiquitous form of basal sliding.

Microseismic stick-slip events often cluster in distinct basal regions, which exhibit frictional properties that favor unstable sliding (Lipovsky et al., 2019; Zoet et al., 2020). In some cases, slip failure occurs successively, giving rise to tremor-type signals (e.g., McBrearty et al., 2020; Winberry et al., 2014) whose frequency peaks are related to the inverse of interevent times (Lipovsky & Dunham, 2016). Such superimposed stick-slip events can account for slip displacement measurable at the ice surface and thus likely play a central role in ice flow. In principle, stick-slip tremor should be easily detectable with conventional on-ice seismometers. However, other sustained cryoseismic sources, in particular englacial water flow, often mask stick-slip tremor (Eibl et al., 2020; McBrearty et al., 2020; Röösli et al., 2014). The manifestation of frictional sliding in the form of microseismic stick-slip tremor may therefore be overlooked.

Here, we present evidence for stick-slip tremor beneath Gornergletscher, a Swiss Alpine glacier. We revisit a microseismic tremor episode, which has previously been classified as a hydraulic process related to the subglacial drainage of a nearby glacier-dammed lake (Heeszel et al., 2014). However, using novel processing of coherent tremor waves, we show that the tremor source is best explained by shear ruptures describing repeated stick-slip motion at the ice-bed interface.

2. Seismic Monitoring and Lake Drainage on Gornergletscher

Located in the Canton Valais, Gornergletscher is Switzerland's second largest glacier, flowing from above 4,500 m to below 2,300 m over a length of about 12 km. The glacier has been continuously retreating over a distance of 3 km since the end of the Little Ice Age in 1870, and to date, the tongue of Gornergletscher is almost exclusively fed by the main tributary Grenzgletscher (GLAMOS, 2017). In the near future, the Gornergletscher tributary is expected to detach entirely from the tongue (Figure 1a).

At the Gornergletscher/Grenzgletscher confluence, lake Gornersee regularly forms with the advent of the melt season. Currently, as a result of sustained surface melt, the lake basin is shallow and poorly defined, extending over several kilometers in the Gornergletscher/Grenzgletscher confluence area (VAW, unpublished information). Until a few years ago, however, the glacier surface formed a basin, which on the western and eastern sides consisted of ice and rock, respectively. The lake basin used to fill with several million cubic meters of water, which typically drained subglacially in June or July over only a few days (Huss et al., 2007; Werder et al., 2009). Such drastic drainages of ice-dammed water bodies result from melt enlargement of englacial and subglacial channels as water dissipates frictional heat when flowing through ice-walled conduits (Roberts et al., 2000).

In 2007, the lake had a volume of 3.7×10^6 m^3 and drainage started on July 4, 2007 as the lake water overspilled into a nearby glacier moulin (Figure 1a, inset). The water discharge accelerated when lake water also found its way into an englacial channel (within ~3 days of initial overspill). The drainage then proceeded over ~2 weeks (July 4–15, 2007), switching between periods of reduced discharge when the lake level dropped beneath an englacial channel entry and periods of accelerated discharge when new fractures established connections to the glacier drainage system (see Werder et al., 2009, for further details on the 2007 drainage). The 2007 drainage was monitored with glaciological measurements (active chemical tracers, surface displacement, and borehole pressure) and an eight-station seismic network (Figure 1a) documented in Werder et al. (2009) and Garcia et al. (2019). Here, we focus on data from six of the eight seismic stations (G7J1, G7J2, G7J4, G7J5, G7J6, and G7J8), which where shallow (<2 m depth) borehole geophones

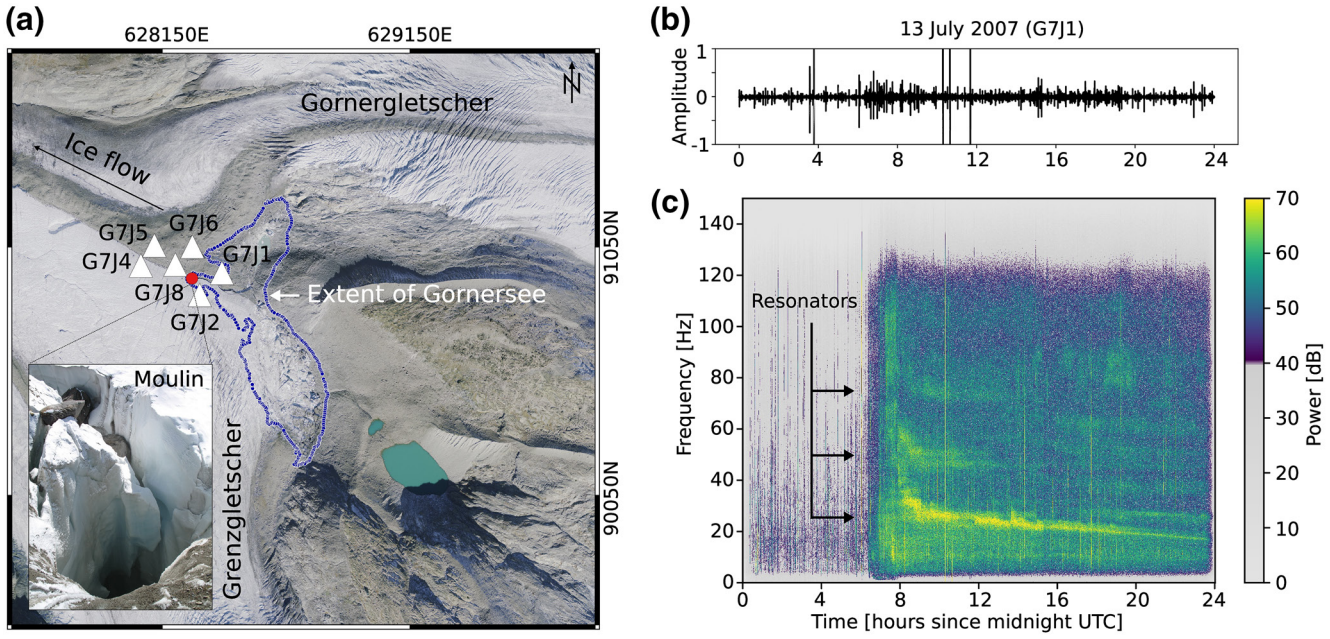

Figure 1. (a) Overview map showing Gornergletscher, Grenzgletscher, and the location of the seismic array (white triangles) used for monitoring lake Gornersee's drainage from May 25 to July 22, 2007 (CH1903 Swiss Grid coordinates. UTM coordinates for station G7J1: 407,410 m Easting, 5,091,352 m Northing [32 T]). The red dot indicates the position of the glacier moulin and the blue line the outline of Gornersee at its highest level in 2007. (b) Day-long seismic record at station G7J1 (band pass filtered between 5 and 45 Hz). (c) Spectrogram at station G7J1 showing the observed harmonic tremor. Spectrogram was computed using a 10-s window with 50% overlap.

with 8 Hz natural frequency. Stations G7J3 and G7J7 were excluded from the analysis as both had a higher natural sensor frequency (28 Hz), which resulted in poor sensitivity to signals analyzed in this study. Moreover, G7J7 was installed at a depth of 122 m.

As in previous years, the 2007 Gornersee drainage affected glacial microseismic activity near the glacier surface and its bed (Garcia et al., 2019; Heeszel et al., 2014; Walter, 2009; Walter et al., 2008). During the 2007 lake drainage, a multihour harmonic tremor signal was discovered on July 13, 2007 (Figures 1b and 1c). The tremor, which was previously interpreted in terms of hydraulic fracture resonances (Heeszel et al., 2014), starts around 07:00 a.m. local time with high energy, about 30 dB above the noise level. Over the course of the day, the energy maximum glides smoothly from higher toward lower frequencies within minutes to hours (Figure 1c). In contrast to the distinct spectral signature, in the time domain, the tremor is hidden in the broadband glacial background noise (Figures 1b and S1).

3. Tremor Analysis

3.1. Matched Field Processing

We analyze the gliding harmonic tremor from July 13, 2007 using signals from the 6.8 Hz sensors. As a generalized beamforming method, we apply matched field processing (MFP) with spherical wave fronts, which yields the location of a seismic noise source by matching the coherent spectra within a sensor network to theoretical spectra called "replica vectors" (see supporting information S1 and Baggeroer et al. [1993] for an overview on MFP). Following previous studies (Walter, 2009; Walter et al., 2015), we assume a homogeneous ice medium for the replica vector calculation.

Conventional MFP assumes that a source emits identical elastic wave phases over the focal sphere in order to match the uniform replica wave polarities. In seismology, this applies to sources whose isotropic moment tensor component dominates over the deviatoric component in the sense that signal polarity is independent of the ray directions of emitted seismic waves (e.g., Julian et al., 1998). Shear ruptures represented by double-couple moment tensors, on the other hand, emit seismic waves, whose polarity depends on the ray

angle with respect to the rupture geometry (Aki & Richards, 2002). Applying conventional MFP to signals from double-couple sources will therefore result in destructive interference between observed signals and replica vectors. This compromises MFP performance and inhibits location by lowering the "beampower," the measure of signal coherence determined by MFP. To account for mixed polarity signals, we propose a polarity optimization by exhaustively testing all combinations of original and inverted signals. This optimization requires an extra step in the grid search: for every geographic grid point Δx, Δy, and Δz and each array element i from M sensors, the trace $d_i(t)$ is multiplied by -1 (or phase shifted by π in the Fourier domain, $d_i(\omega)$). If stacking the inverted trace leads to a higher beampower (Equation 3, supporting information), the trace is considered "inverted." For the "correct" polarity combination of all traces, the MFP beampower is maximized, that is, we have optimized the MFP. In such a routine, the MFP output is optimized iteratively for every station at each grid point by flipping stations with polarities opposite to the replica vector. Finally, double-couple sources can be located properly and the optimization can actually define the radiation pattern for the rupture geometry (supporting information S3 and Figure S2).

3.2. MFP Implementation

Vertical-component seismic data on July 12 and 13, 2007 were band pass filtered between 15 and 25 Hz using a second-order Butterworth filter and processed with MFP applied to a 15-min sliding window. Each 15 min observation period is split into 1 min subwindows, whose amplitudes are normalized with respect to the traces maxima. The subwindows are then used to calculate the average stack of the cross-spectral density matrix for the observation period (supporting information S1 and Equation 1). The array geometry limits the analysis to a minimum wavelength of 160 m, based on the theoretical array response defined by Wathelet et al. (2008) (Figure S3). Assuming an S wave velocity of 1,800 m/s yields a high-frequency limit of 11.25 Hz for array analysis, whereas the tremor shows high energy between 20 and 35 Hz. We chose the band of 15–25 Hz for our analysis because lower frequencies (5–15 Hz) lack energy and clear phase onsets in cross correlations (Figure S4), while higher frequencies are too far from the resolvable range considering the theoretical array response. In order to suppress side lobes in the MFP due to spatial aliasing, we stack MFPs for 50 equally spaced frequencies over the 15–25 Hz band. As the location of the side lobes in the MFP output is frequency dependent, the stacking suppresses the side lobes and amplifies the true maximum, which is not frequency dependent in a homogeneous medium (Kværna & Doornbos, 1986). This is confirmed by synthetic tests based on elastic wavefield modeling showing that our array is indeed capable of correctly locating 15–25 Hz signals (supporting information S2 and Figure S5). Moreover, source locations for the 15–25 Hz band cluster in space compared to lower or higher frequencies. These locations seem to be fairly well resolved, even up to 30 Hz, regarding the beampower, while a resolution loss is indicated above 30 Hz (Figure S6).

The MFP grid spacing was set to Δx, Δy, and $\Delta z = 5$ m, the grid dimensions to $700 \times 700 \times 250$ m (x, y, z) with the array centered at the surface. An additional inversion for the seismic velocity was bound by $c_{\min} = 1{,}600$ m/s (slightly below Rayleigh wave velocity in ice) and $c_{\max} = 2{,}000$ m/s (slightly above S wave velocity in ice, Podolskiy & Walter, 2016) and using increments of 10 m/s. MFP was first computed in the conventional way using the phase-match replica and the Bartlett processor (Equations 2 and 3 in the supporting information) and MFP polarity optimization in a second step. The optimization procedure is demonstrated in the time domain for one exemplary short-duration impulsive tremor signal (display window of 2 s) in Figure 2.

4. Results and Discussion

The epicenters derived from the conventional MFP and the MFP polarity optimization are presented in Figures 3a and 3b) (and overlain in Figure 3c) and are color coded with respect to their time window with hour 0 corresponding to 07:00 a.m. on July 13, 2007 (for source depth and velocity color-codes, see Figure S7). Prior to the tremor onset (gray scale), conventional MFP leads to source locations that form small local clusters at the surface of the glacier. In the very beginning of the tremor (hour 0), the sources form a linear feature to the northwest of the array. Near the end of the tremor, a cluster of sources in the central part of the array evolves. These locations range in depth between 0 and 150 m. In addition to these larger clusters, smaller local clusters mostly occur in the near-surface environment of the array. However, the linear

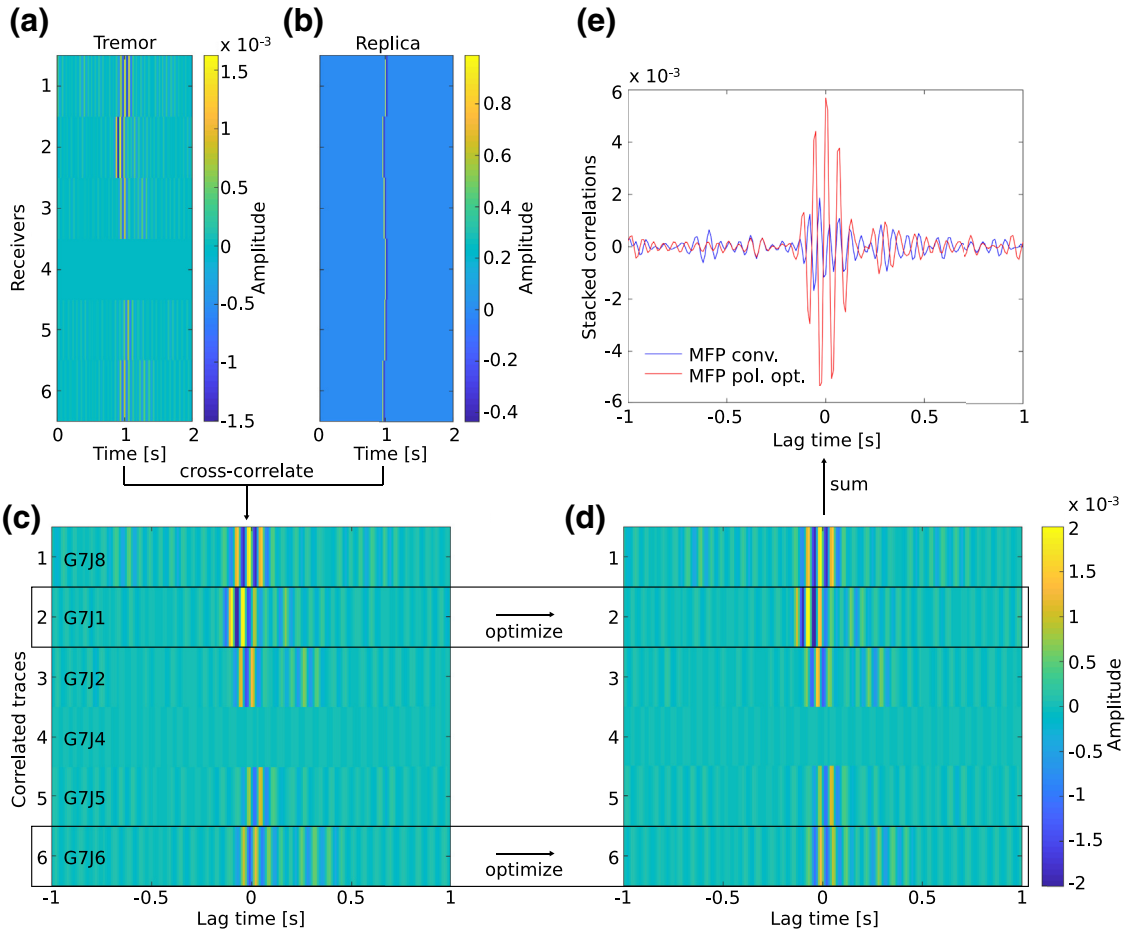

Figure 2. MFP polarity optimization for one stack (1 min) during one observation period (10:00–10:15 a.m. on July 13, 2007) during the tremor occurrence. (a) Exemplary tremor signal (display window of 2 s) within one stack. The stack was band pass filtered between 15 and 25 Hz using a second-order Butterworth filter and normalized to the amplitude maximum. Sensor 4 (G7J4) was lacking data during the display window. (b) Synthetic replica vector computed for the source location of the MFP maximum of the respective observation period at $x, y, z = 595, 600, 150$ m and velocity $c = 1{,}770$ m/s. (c) Cross correlation of (a) and (b). (d) MFP polarity optimization (see supporting information for synthetic example, Figure S2). The polarity of two stations (G7J1, G7J6) was flipped to enhance the MFP beampower. (e) Comparison of the beampower (stacked cross-correlation functions) of conventional MFP (c) in blue and MFP polarity optimization (d) in red. MFP, matched field processing.

feature moves to a depth of about 60–80 m over time. Lastly, the central cluster contains both shallow and deep sources down to 150 m. The velocity generally ranges between 1,620 and 1,760 m/s, with most of the sources having velocities within the lower two thirds of this range (Figure S8). Shallow clusters are mostly characterized by lower velocities, while deeper clusters (especially the one in the central part of the array) have values up to 1,760 m/s. This is likely related to the MFP being dominated by strong Rayleigh waves for the shallow events, which travel at around 92% of the shear wave velocity in a homogeneous medium (Aki & Richards, 2002).

In contrast to conventional MFP, MFP polarity optimization indicates a large cluster of sources to the northeast (NE) of the array during most of the tremor period. Before (gray) and at the very end of the tremor (shades of dark blue), the sources scatter across the array, forming small local clusters as well as contributing to a central cluster, which was also observed with conventional MFP. All sources range in depth between 0 and 250 m, with the NE cluster predominantly characterized by greater depths between 150 and 250 m. The velocities are generally higher within the cluster as well. They mostly lie around 1,760 m/s and reach up to 1,820 m/s. Most other sources located near the glacier surface are characterized by velocities between 1,630 and 1,760 m/s. In the following, we will refer to the sources clustering to the NE and characterized by high velocities, as well as greater source depth, as "the tremor cluster" (July 13, 2007, 07:00 a.m.–05:00

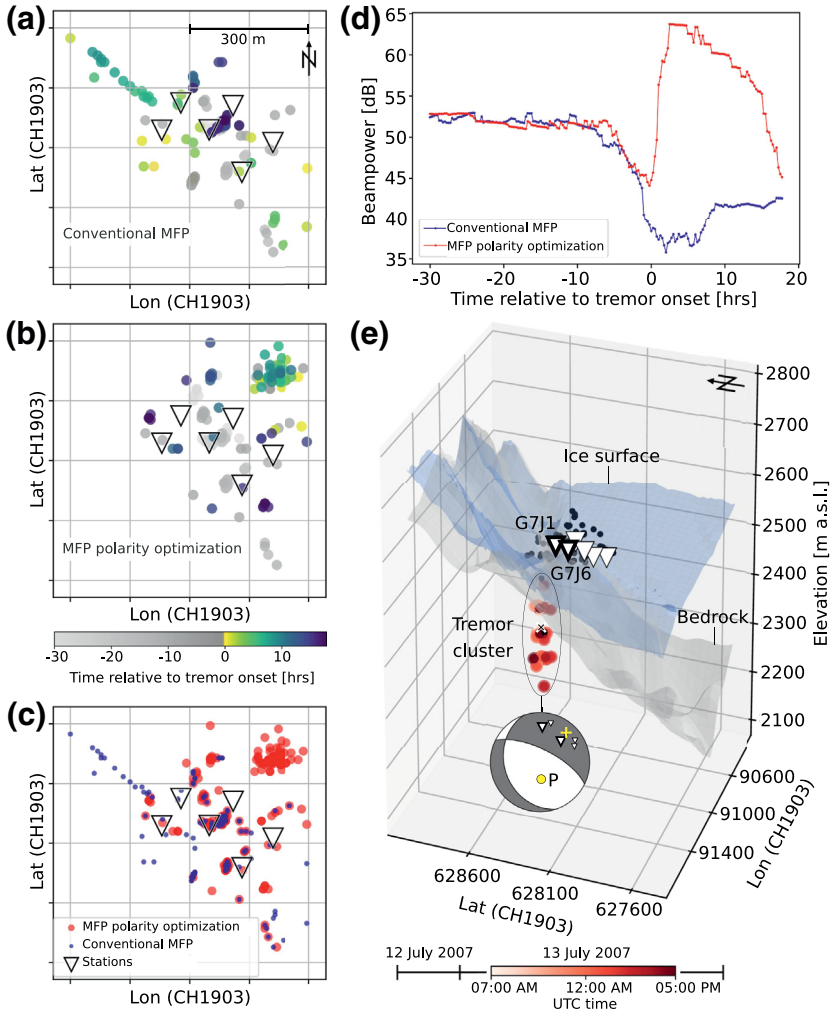

Figure 3. Source location maps from conventional MFP (a) and MFP polarity optimization (b); dots represent source locations (beampower maximum) of one observation period (15 min) during 2 days (July 12 and 13, 2007), 192 observation windows in total. Epicenters are color coded with respect to their time window with hour 0 being at 07:00 a.m., July 13, 2007; triangles represent seismic stations. (c) Epicenters derived from conventional MFP (blue) and MFP polarity optimization (red). (d) Beampower as a function of time of the epicenters displayed in (c). (e) Source locations from MFP polarity optimization plotted together with the ice surface (blue) and the bedrock topography (gray). Tremor cluster locations (July 13, 2007, 07:00 a.m.–05:00 p.m., 40 observation windows) are color coded by time in shades of red; the remaining 152 locations before and after the tremor are indicated by black dots (shallow depths). Triangles represent seismic stations with G7J1 and G7J6 (bold outline) being the inverted stations, that is, the polarity was flipped for 35 of the 40 observation windows during the tremor (87.5%, Figure 2). The beach ball shows the *P* wave radiation for the focal mechanism derived from the ice flow direction and the bedrock topography, independent of the seismic data (supporting information S4 and Figure S10) assuming stick-slip motion at the average tremor cluster location (black X). Dot and cross (yellow) show the two nodal points coinciding with the pressure and tension axes of the moment tensor. Near these points, polarity changes of *S* waves are expected (see main text for details). MFP, matched field processing.

p.m., 40 observation windows). For 35 of the 40 observation windows (87.5%), we observe the same polarity optimization with inverted polarities at stations G7J1 and G7J6 (Figure 2).

The epicentral locations of conventional MFP and MFP polarity optimization are similar for about two-thirds of the considered time span. However, clear differences exist during the tremor occurrence with sources from conventional MFP predominantly clustering toward the NW (linear feature) and sources from MFP polarity optimization clustering toward the NE ("tremor cluster," Figure 3c). Figure 3d compares the evolution of the beampower; a similar trend in beampower is observed before the tremor. However, following the onset of the tremor (hour 0), the conventional MFP beampower decreases from ~52 dB down

to 35 dB, while the beampower of MFP with polarity optimization increases substantially to ~64 dB. This observation indicates that constructive interference of the waveforms occurs in the polarity optimization MFP. In addition to the increased beampower, the tremor sources cluster near or below the bed (Figure 3e). The averaged coordinates of the cluster (black X) are 628,395, 91,182, and 2,402 m a.s.l. (northing, easting, and height above sea level of CH1903 Swiss Grid coordinate system), which is situated about 114 m beneath the ice surface and 30 m beneath the estimated bedrock.

The two most important findings among these observations are (1) the optimized MFP analysis identifies different polarities for stations G7J1 and G7J6 in the tremor cluster signal and the beampower for these flipped polarity solutions is substantially enhanced with respect to the conventional MFP algorithm. (2) The optimized MFP locates the tremor cluster close to the ice-rock interface, specifically to within 30 m of the radar-derived bed. We now tie these findings into further observations to argue for a stick-slip mechanism rather than the hydraulic resonance previously suggested (Heeszel et al., 2014).

The spectral signature supports the stick-slip interpretation of the tremor cluster: as predicted by theory (Lipovsky & Dunham, 2016), three dominant resonances near 25, 50, and 75 Hz are evenly spaced near the tremor onset (Figure 1c). In contrast, hydraulic resonance frequencies f_n, where n is the overtone index, tend to follow a nonlinear relation $f_n \,/\, f_1 = n^{\frac{3}{2}}$ (Lipovsky & Dunham, 2015). The same argument was employed by Schöpa et al. (2018) to distinguish stick-slip tremor during the Askja caldera landslide in Iceland in 2014 from fluid-induced resonances. In addition, hydraulic tremors have sources with strong isotropic components (Röösli et al., 2016), whose signals reside at lower frequencies than those observed in this article (Gimbert et al., 2014, 2016; Röösli et al., 2014) and are therefore an unlikely explanation of this tremor.

We next determine the polarization of the coherent signals, which our MFP algorithm optimizes to determine variations in tremor signal polarity. First, the horizontal components of the borehole sensors are aligned using linearly polarized *P* waves of surface crevasse icequakes that have been located based on surface waves (Garcia et al., 2019). We used 10 events, which occurred within 1–2 days of the tremor episode and do not observe systematic drifts in geographical orientation of the horizontal axes, which would be indicative of sensor rotation within a vertical borehole shaft. Then, following Haney et al. (2020), we estimate the frequency-dependent polarization of tremor signals at each station. This analysis indicates high rectilinearity and low ellipticity for the dominant frequencies during the tremor, in agreement with linearly polarized body waves originating from a stick-slip source (Figure S9). Moreover, the velocities of around 1,800 m/s estimated from MFP polarity optimization are in close agreement with previous *S* wave velocity estimates on Gornergletscher (Walter, 2009). Thus, we conclude that the dominant tremor signal consists of linearly polarized *S* waves.

The observation of dominant *S* waves implies that the moment tensor representing the tremor source has a strong deviatoric component, since purely isotropic moment tensors radiate *P* waves exclusively. In addition, the optimized MFP analysis determines mixed polarities within the network. This means that the radiation pattern of the deviatoric moment tensor component must produce a nodal plane or nodal point, which induces *S* waves whose polarity at G7J1 and G7J6 is opposite compared to the other stations.

In case of a glacier-hydraulic tremor, two moment tensors are reasonable and both have positive entries, only, in their diagonalized form: water resonance within a cylindrical conduit (Röösli et al., 2016) and a tensile crack representing a fracture resonance (Julian et al., 1998; Lipovsky & Dunham, 2016). Geometric orientations of these two resonance bodies are difficult to constrain, as both horizontal and vertical orientations for englacial conduits (Roberts et al., 2000; Röösli et al., 2016) and tensile fractures (Harper et al., 2010; Walter et al., 2010) are possible. Consequently, the moment tensor and its deviatoric component giving nodal planes or points, which would explain polarity flips, are difficult to guess for glacier-hydraulic resonances.

In contrast to a hydraulic resonance, stick-slip geometry arises naturally when assuming that the fault planes are bed-parallel and slip is in the ice sliding direction (Zoet et al., 2012). At the tremor hypocenter, we determine this stick-slip geometry using bedrock topography derived from radio echo sounding (Huss, 2005; Sugiyama et al., 2008) and basal slip calculated with an ice flow model of Gornergletscher (Riesen et al., 2010). This results in the double-couple moment tensor with strike = 161° (measured clockwise from north),

dip = 29°, and rake = −49° shown in Figure 3e (see Figure S10 for details on the derivation). As for any double-couple source, the *S* wave radiation pattern of this mechanism has two nodal points coinciding with the pressure and tension axes of the moment tensor (Figure 4.6 in Aki & Richards, 2002). Stations projecting on opposite sides of these nodal points on the focal sphere will have opposite S-polarization. In the case of our derived double-couple mechanism representing bed-parallel sliding, the focal point of the tension axis projects directly into the seismic network (Figure 3e) and may thus explain the observed mixed polarities (flip at G7J1 and G7J6).

The local rupture direction during stick-slip faulting may deviate to some extent from the overall ice flow direction (Anandakrishnan & Bentley, 1993). However, the projection of the focal point within the network argues for a double-couple source as an explanation for the observed polarity flip within the seismic network. Furthermore, the deviatoric moment tensor component of hydraulic conduit or crack resonances is likely dominated by the isotropic component. For example, for the tensile crack, the deviatoric compensated linear vector dipole (CLVD) component also emits mixed S-polarities, but for ice, the isotropic component is nearly 5 times larger than the deviatoric CLVD (Walter et al., 2013). This suggests that a crack source emits substantially more *P* wave energy than a purely deviatoric double-couple moment tensor representing stick-slip. Our observation of dominant *S* wave energy therefore favors a stick-slip source over a tensile crack mechanism.

5. Conclusion

The investigated microseismic tremor is consistent with a basal source beneath Gornergletscher, Switzerland. The time-evolving spectral signature of the tremor points toward a repeating stick-slip mechanism rather than a hydraulic resonance. The stick-slip mechanism is also consistent with observed variations in signal polarity, bedrock geometry, and basal sliding direction.

Generally, under velocity weakening conditions, frictional sliding can result in sliding instabilities, which manifest themselves in discrete rupture events or stick-slip tremor such as found here (Lipovsky & Dunham, 2016). Beneath Antarctica's fast flowing Whillans Ice Stream, stick-slip tremor accompanies regular large-scale slip episodes, during which the ice stream undergoes most of its displacement (Winberry et al., 2013). No such surging behavior was observed for the tremor presented in this study as ice velocities measured at several coordinates on Gornergletscher's surface (Garcia et al., 2019) did not reveal an anomaly such as a widespread or unusually large flow acceleration (Figure S11). Our tremor seems more similar to recent observations at a Greenland ice stream, where stable or discrete stick-slip sliding transitions into stick-slip tremor (McBrearty et al., 2020). The authors of the Greenland study explain such transitions in terms of strain imbalances or pore water pressure changes at the ice stream bed. These mechanisms could also explain the transient nature of the stick-slip tremor of the present study. Subglacial pressure changes, in particular, seem a natural explanation in view of the concurrent drainage of lake Gornersee.

The nondetection of large-scale ice flow anomalies furthermore suggests that our stick-slip tremor is a local phenomenon of a spatially limited bed region ("sticky spot"), where strain is accumulated and released in the form of successive stick-slip failure. To test the hypothesis that the tremor episode investigated here was not only a fortuitous observation, analysis of more tremor signals is needed, ideally using networks with more sensors and larger apertures (Sergeant et al., 2020). Alternatively, deep borehole seismometers installed in the vicinity of the glacier bed may contain records of stick-slip tremors, whose signals are too weak to be detected at the surface. Confirmation of our hypothesis would be another piece of evidence for ubiquitous seismogenic sliding, whose underlying physics are rooted in frictional processes rather than slow ice and bed deformation proposed in traditional theories.

Acknowledgments
We thank VAW and its personnel for fieldwork support on Gornergletscher and for making the 2007 Gornersee outlines available to this study. Seismometer data of the 4D local glacier seismology network (https://doi.org/10.12686/sed/networks/4d) are archived at the Swiss Seismological Service and can be accessed via its web interface http://arclink.ethz.ch/webinterface/. The salary of F. Walter was financed by the Swiss National Science Foundation via grant PP00P2_183719.

References

Aki, K., & Richards, P. (2002). *Quantitative seismology* (2nd ed.). Sausalito: University Science Books.
Alley, R., Clark, P., Huybrechts, P., & Joughin, I. (2005). Ice-sheet and sea-level changes. *Science*, *310*, 456–460.
Anandakrishnan, S., & Bentley, C. (1993). Micro-earthquakes beneath Ice Streams B and C, West Antarctica: Observations and implications. *Journal of Glaciology*, *39*(133), 455–462.
Aster, R., & Winberry, R. (2017). Glacial seismology. *Reports on Progress in Physics*, *80*, 126801.
Baggeroer, A., Fellow, I. E. E. E., Kuperman, W., & Mikhalevsky, P. (1993). An overview of matched field methods in ocean acoustics. *IEEE Journal of Oceanic Engineering*, *18*(4), 401–424.

Bartholomew, I., Nienow, P., Mair, D., Hubbard, A., King, M., & Sole, A. (2010). Seasonal evolution of subglacial drainage and acceleration in a Greenland outlet glacier. *Nature Geoscience*, *3*, 408–411.
Bougamont, M., Christoffersen, P., Hubbard, A., Fitzpatrick, A., Doyle, S., & Carter, S. (2014). Sensitive response of the Greenland ice sheet to surface melt drainage over a soft bed. *Nature Communications*, *5*, 5052.
Clarke, G. (1987). A short history of scientific investigations on glaciers. *Journal of Glaciology*, *33*, 4–24.
Conway, H., Catania, G., Raymond, C., Gades, A., Scambos, T., & Engelhardt, H. (2002). Switch of flow direction in an Antarctic ice stream. *Nature*, *419*, 465–467.
Eibl, E., Bean, C., Einarsson, B., Pàlsson, F., & Vogfjörd, K. (2020). Seismic ground vibrations give advanced early-warning of subglacial floods. *Nature Communications*, *11*(1), 1–11.
Engelhardt, H., & Kamb, B. (1998). Basal sliding of Ice Stream B, West Antarctica. *Journal of Glaciology*, *44*(147), 223–230.
Faillettaz, J., Funk, M., & Vincent, C. (2015). Avalanching glacier instabilities: Review on processes and early warning perspectives. *Reviews of Geophysics*, *53*, 203–224. https://doi.org/10.1002/2014RG000466
Gagliardini, O., Cohen, D., Råback, P., & Zwinger, T. (2007). Finite-element modeling of subglacial cavities and related friction law. *Journal of Geophysical Research*, *112*, F02027. https://doi.org/10.1029/2006JF000576
Garcia, L., Luttrell, K., Kilb, D., & Walter, F. (2019). Joint geodetic and seismic analysis of surface crevassing near a seasonal glacier-dammed lake at Gornergletscher, Switzerland. *Annals of Glaciology*, *60*(79), 1–13.
Gimbert, F., Tsai, V., Amundson, J., Bartholomaus, T., & Walter, J. (2016). Subseasonal changes observed in subglacial channel pressure, size, and sediment transport. *Geophysical Research Letters*, *43*, 3786–3794. https://doi.org/10.1002/2016GL068337
Gimbert, F., Tsai, V., & Lamb, M. (2014). A physical model for seismic noise generation by turbulent flow in rivers. *Journal of Geophysical Research: Earth Surface*, *119*, 2209–2238. https://doi.org/10.1002/2014JF003201
GLAMOS (2017). The Swiss Glaciers 2013/14 and 2014/15. In A. Bauder (Ed.), *Glaciological Report No. 135/136 of the Cryospheric Commission (EKK) of the Swiss Academy of Sciences (SCNAT)*. Bern, Switzerland: VAW / ETH Zürich. Retrieved from https://doi.org/10.18752/glrep_135-136
Haney, M., Fee, D., McKee, K., Lyons, J., Matoza, R., Wech, A., et al. (2020). Co-eruptive tremor from Bogoslof volcano: Seismic wavefield composition at regional distances. *Bulletin of Volcanology*, *82*(18), 1–14.
Harper, J., Bradford, J., Humphrey, N., & Meierbacktol, T. (2010). Vertical extension of the subglacial drainage system into basal crevasses. *Nature*, *467*, 579–582.
Harper, J., Humphrey, N., Pfeffer, W., & Lazar, B. (2007). Two modes of accelerated glacier sliding related to water. *Geophysical Research Letters*, *34*, L12503. https://doi.org/10.1029/2007GL030233
Heeszel, D., Walter, F., & Kilb, D. (2014). Humming glaciers. *Geology*, *42*(12), 1099–1102.
Helmstetter, A., Nicolas, B., Comon, P., & Gay, M. (2015). Basal icequakes recorded beneath an Alpine glacier (Glacier d'Argentière, Mont Blanc, France): Evidence for stick-slip motion? *Journal of Geophysical Research: Earth Surface*, *120*, 379–401. https://doi.org/10.1002/2014JF003288
Huss, M. (2005). *Gornergletscher: Gletscherseeausbrüche und Massenbilanzabschätzungen (in German with English abstract) (dissertation)*. ETH Zurich.
Huss, M., Bauder, A., Werder, M., Funk, M., & Hoch, R. (2007). Glacier-dammed lake outburst events of Gornersee, Switzerland. *Journal of Glaciology*, *53*, 189–200.
Huybrechts, P. (2002). Sea-level changes at the LGM from ice-dynamic reconstructions of the Greenland and Antarctic ice sheets during the glacial cycles. *Quaternary Science Reviews*, *21*, 203–231.
Iken, A. (1981). The effect of the subglacial water pressure on the sliding velocity of a glacier in an idealized numerical model. *Journal of Glaciology*, *27*(97), 407–421.
Iverson, N. (2010). Shear resistance and continuity of subglacial till: Does hydrology trump rheology? *Journal of Glaciology*, *56*(200), 1104–1114.
Iverson, N., Coen, D., Hooyer, T., Fischer, U., Jackson, M., Moore, P., & Kohler, J. (2003). Effects of basal debris on glacier flow. *Science*, *301*, 81–84.
Julian, B., Miller, A., & Foulger, G. (1998). Non-double-couple earthquakes. *Reviews of Geophysics*, *36*(4), 525–549.
Kääb, A., Leinss, S., Gilbert, A., Bühler, Y., Gascoin, S., Evans, S., & Yao, T. (2018). Massive collapse of two glaciers in western Tibet in 2016 after surge-like instability. *Nature Geoscience*, *11*, 114–123.
Kværna, T., & Doornbos, D. (1986). *An integrated approach to slowness analysis with arrays and three-component stations*. (NORSAR Scientific Report 2–85/86, pp. 60–69). Kjeller, Norway: NORSAR.
Lipovsky, B., & Dunham, E. (2015). Vibrational modes of hydraulic fractures: Inference of fracture geometry from resonant frequencies and attenuation. *Journal of Geophysical Research: Solid Earth*, *120*, 1080–1107. https://doi.org/10.1002/2014JB011286
Lipovsky, B., & Dunham, E. (2016). Tremor during ice-stream stick slip. *The Cryosphere*, *10*, 385–399.
Lipovsky, B., Meyer, C., Zoet, L., McCarthy, C., Hansen, D., Rempel, A., & Gimbert, F. (2019). Glacier sliding, seismicity and sediment entrainment. *Annals of Glaciology*, *60*(79), 182–192.
Maier, N., Humphrey, N., Harper, J., & Meierbachtol, T. (2019). Sliding dominates slow-flowing margin regions, Greenland Ice Sheet. *Science Advances*, *5*(7), 1–10.
McBrearty, I., Zoet, L., & Anandakrishnan, S. (2020). Basal seismicity of the Northeast Greenland Ice Stream. *Journal of Glaciology*, *66*, 430–446.
Meier, M., Dyurgerov, M., Rick, U., O'Neel, S., Pfeffer, W., Anderson, R., & Glazovsky, A. (2007). Glaciers dominate eustatic sea-level rise in the 21st century. *Science*, *317*, 1064–1067.
Podolskiy, E., & Walter, F. (2016). Cryoseismology. *Reviews of Geophysics*, *54*, 708–758. https://doi.org/10.1002/2016RG000526
Riesen, P., Sugiyama, S., & Funk, M. (2010). The influence of the presence and drainage of an ice-marginal lake on the flow of Gornergletscher, Switzerland. *Journal of Glaciology*, *56*(196), 278–286.
Ritz, C., Edwards, T., Durand, G., Payne, A. J., Peyaud, V., & Hindmarsh, R. (2015). Potential sea-level rise from Antarctic ice-sheet instability constrained by observations. *Nature*, *528*, 115–118.
Roberts, M., Russell, A., Tweed, F., & Knudsen, O. (2000). Ice fracturing during Jökulhlaups: Implications for englacial floodwater routing and outlet development. *Earth Surface Processes and Landforms*, *25*, 1429–1446.
Röösli, C., Walter, F., Ampuero, J.-P., & Kissling, E. (2016). Seismic Moulin tremor. *Journal of Geophysical Research: Earth Surface*, *121*, 5838–5858. https://doi.org/10.1002/2015JB012786
Röösli, C., Walter, F., Husen, S., Andrews, L., Lüthi, M., Catania, G., & Kissling, E. (2014). Sustained seismic tremors and icequakes detected in the ablation zone of the Greenland Ice Sheet. *Journal of Glaciology*, *60*(221), 563–575.

Schoof, C. (2005). The effect of cavitation on glacier sliding. *Proceedings of the Royal Society*, *461*, 609–627.
Schöpa, A., Chao, W., Lipovsky, B., Hovius, N., White, R., Green, R., & Turowsky, J. (2018). Dynamics of the Askja caldera July 2014 landslide, Iceland, from seismic signal analysis: Precursor, motion, aftermath. *Earth Surface Dynamics*, *6*, 467–485.
Sergeant, A., Chmiel, M., Lindner, F., Walter, F., Roux, P., Chaput, J., & Mordret, A. (2020). On the Green's function emergence from interferometry of seismic wave fields generated in high-melt glaciers: Implications for passive imaging and monitoring. *The Cryosphere*, *14*(3), 1139–1171.
Sugiyama, S., Bauder, A., Huss, M., Riesen, P., & Funk, M. (2008). Triggering and drainage mechanisms of the 2004 glacier-dammed lake outburst in Gornergletscher, Switzerland. *Journal of Geophysical Research*, *113*, F04019. https://doi.org/10.1029/2007JF000920
Tulaczyk, S. (1999). Ice sliding over weak, fine-grained tills: Dependence of ice-till interactions on till granulometry. *Glacial Processes. Past and Modern: Boulder, Colorado, Geological Society of America Special Paper*, *337*, 159–177.
Walter, F. (2009). *Seismic activity on Gornergletscher during Gornersee Outburst Floods*. (dissertation, DISS ETH NO. 18184). ETH Zurich.
Walter, F., Canassy, P., Husen, S., & Clinton, J. (2013). Deep icequakes: What happens at the base of Alpine glaciers? *Journal of Geophysical Research: Earth Surface*, *118*, 1720–1728. https://doi.org/10.1002/jgrf.20124
Walter, F., Chaput, J., & Luthi, M. (2014). Thick sediments beneath Greenland's ablation zone and their potential role in future ice sheet dynamics. *Geology*, *42*, 487–490.
Walter, F., Deichmann, N., & Funk, M. (2008). Basal icequakes during changing subglacial water pressures beneath Gornergletscher, Switzerland. *Journal of Glaciology*, *54*(186), 511–521.
Walter, F., Dreger, D., Clinton, J., Deichmann, N., & Funk, M. (2010). Evidence for near-horizontal tensile faulting at the base of Gornergletscher, a Swiss Alpine glacier. *Bulletin of the Seismological Society of America*, *100*(2), 458–472.
Walter, F., Gräff, D., Lindner, F., Paitz, P., Köpfli, M., Chmiel, M., & Fichtner, A. (2020). Distributed acoustic sensing of microseismic sources and wave propagation in glaciated terrain. *Nature Communications*, *11*(2436), 1–10.
Walter, F., Roux, P., Röösli, C., Lecointre, A., Kilb, D., & Roux, P. (2015). Using glacier seismicity for phase velocity measurements and Green's function retrieval. *Geophysical Journal International*, *201*, 1722–1737.
Wathelet, M., Jongmans, D., Ohrnberger, M., & Bonnefoy-Claudet, S. (2008). Array performances for ambient vibrations on a shallow structure and consequences over V s inversion. *Journal of Seismology*, *12*(1), 1–19.
Weertman, J. (1957). On the sliding of glaciers. *Journal of Glaciology*, *3*(21), 33–38.
Werder, M., Loye, A., & Funk, M. (2009). Dye tracing a jokulhlaup: I. Subglacial water transit speed and water-storage mechanism. *Journal of Glaciology*, *55*(193), 889–898.
Wiens, D., Anandakrishnan, S., Winberry, J., & King, M. (2008). Simultaneous teleseismic and geodetic observations of the stick-slip motion of an Antarctic ice stream. *Nature*, *453*, 770–775.
Winberry, J., Anandakrishnan, S., Alley, R., Wiens, D., & Pratt, M. (2014). Tidal pacing, skipped slips and the slowdown of Whillans Ice Stream, Antarctica. *Journal of Glaciology*, *60*(222), 795–807.
Winberry, J., Anandakrishnan, S., Wiens, D., & Alley, R. (2013). Nucleation and seismic tremor associated with the glacial earthquakes of Whillans Ice Stream, Antarctica. *Geophysical Research Letters*, *40*, 312–315. https://doi.org/10.1002/grl.50130
Zoet, L., Anandakrishnan, S., Alley, R., Nyblade, A. A., & Wiens, D. (2012). Motion of an Antarctic glacier by repeated tidally modulated earthquakes. *Nature Geoscience*, *5*(9), 623–626.
Zoet, L., Ikari, M., Alley, R., Marone, C., Anandakrishnan, S., Carpenter, B., & Scuderi, M. (2020). Application of constitutive friction laws to glacier seismicity. *Geophysical Research Letters*, *47*, e2020GL088964. https://doi.org/10.1029/2020GL088964
Zoet, L., & Iverson, N. (2020). A slip law for glaciers on deformable beds. *Science*, *368*(6486), 76–78.